European Journal of Orthodontics, 2021, 698–707
doi:10.1093/ejo/cjab043
Advance Access publication 1 July 2021

Original article

mRNA and long non-coding RNA expression profiling of human periodontal ligament cells under tension loading

Yifan Lin[1], Tianfan Cheng[2], Shaoyue Zhu[1], Min Gu[1], Lijian Jin[2] and Yanqi Yang[1]

[1]Division of Paediatric Dentistry and Orthodontics, Faculty of Dentistry, The University of Hong Kong, Hong Kong SAR, China, [2]Division of Periodontology and Implant Dentistry, Faculty of Dentistry, The University of Hong Kong, Hong Kong SAR, China

Correspondence to: Yanqi Yang, Orthodontics, Prince Philip Dental Hospital, No. 34 Hospital Road, Hong Kong SAR, China. E-mail: yangyanq@hku.hk

Summary

Objective: This study explored the expression profiles of messenger RNAs (mRNAs) and long non-coding RNAs (lncRNAs) in human periodontal ligament (PDL) cells subjected to tensile loading.
Methods: PDL cells were isolated from the teeth of five healthy individuals, cultured and then exposed to tensile loading. RNA sequencing was performed to explore the mRNA and lncRNA expression profiles with or without tensile loading. Differential expression, Gene Ontology (GO) and Kyoto Encyclopedia of Genes and Genomes (KEGG) enrichment analyses were conducted to reveal enriched biological functions and signal transduction pathways. Quantitative polymerase chain reaction (qPCR) was performed to validate the expression of specific mRNAs and lncRNAs associated with the enriched pathways.
Results: Tensile loading significantly enhanced the osteogenic potential of PDL cells. Overall, 1438 mRNAs (860 up- and 578 down-regulated) and 195 lncRNAs (107 up- and 88 down-regulated) were differentially expressed (adjusted *P*-value <0.05) in the tensile loading group versus the control group. GO and KEGG analyses of the differentially expressed genes indicated significant enrichment in osteogenesis-related biological processes and intracellular signal transduction pathways (e.g. the PI3K–Akt pathway), respectively. The qPCR analysis validated the expression levels of five selected mRNAs (*EGFR*, *FGF5*, *VEGFA*, *HIF1A*, and *FOXO1*) and three selected lncRNAs (*CYTOR*, *MIR22HG*, and *SNHG3*).
Limitation: Further studies are warranted to validate the mechanisms regulating tension-induced bone remodelling in PDL cells and potential regulation by the identified lncRNAs.
Conclusion: The notably altered mRNA and lncRNA expression profiles in PDL cells under tensile loading enhance our mechanistic understanding of tension-induced osteogenesis.

Introduction

Orthodontic tooth movement (OTM) is a unique mechanical load-mediated process of bone and periodontal tissue remodelling. The periodontal ligament (PDL) is located between the tooth and alveolar bone, where it serves as the target of stress loading and plays a critical role in tension-induced bone formation and compression-induced bone resorption (1). The PDL has a regenerative capacity. Specifically, PDL cells exhibit 'stemness' (i.e. stem-cell likeness) and can differentiate into various types of tissue, including the PDL, cementum, and alveolar bone. PDL cells are load sensitive, and their proliferative and osteogenic potentials increase with stimulation under appropriate loading levels (2–4).

Ribonucleic acid (RNA) is the most versatile biomolecule. Two categories of RNA have been identified, namely protein-coding (coding) and non-protein-coding (non-coding) RNA (5). The latter RNAs typically regulate gene expression but are not translated into proteins. Non-coding RNAs can be further subdivided into two major groups based on their length: short non-coding RNAs and long non-coding RNAs (lncRNAs, >200 nucleotides). LncRNAs comprise a large and diverse class of transcribed RNA molecules with the capacity to regulate gene expression at both the transcriptional and translational levels in various biological processes (6).

Reports have suggested that lncRNAs are involved in osteogenesis in PDL cells. Specifically, He *et al*. revealed that the lncRNA taurine-upregulated gene1 (*TUG1*) promoted osteogenesis by activating lin-28 homologue A, an RNA-binding protein (7). In addition to regulating messenger RNAs (mRNAs) through independent mechanisms, lncRNAs can act as microRNA sponges by competitively binding to these molecules through microRNA response elements (8, 9). This binding attenuates the ability of microRNAs to down-regulate mRNA expression and thus indirectly regulates mRNA expression. Gu *et al*. identified two lncRNAs (*TCONS_00212979* and *TCONS_00212984*) in PDL cells that interact with microRNAs to regulate osteogenesis via the mitogen-activated protein kinase pathway (10). Furthermore, Peng *et al*. showed that lncRNA-ANCR attenuated osteogenesis in PDL cells by sponging *microRNA-758* (11).

A recent report demonstrated that mechanical loading could affect lncRNA expression profiles (12). In that study, high-throughput sequencing was used to demonstrate significant changes in lncRNA expression patterns in response to compressive loading (12). This observation has contributed greatly to our understanding of mechanical loading-induced bone remodelling. Additionally, tensile loading has been reported to induce osteogenesis and promote bone formation in PDL cells (13, 14). Still, the process by which lncRNAs respond to tensile loading and the intracellular signalling pathways involved in tension-induced osteogenesis in PDL cells have not been thoroughly studied.

This study was conducted to explore changes in the mRNA and lncRNA expression profiles of PDL cells under tensile loading. The cells were subjected to high-throughput RNA sequencing (RNA-seq), and Gene Ontology (GO) and Kyoto Encyclopedia of Genes and Genomes (KEGG) pathway analyses were used to explore the enriched functions and potential regulatory pathways among the differentially expressed genes between cells in the presence or absence of tensile loading. Furthermore, the expression levels of certain lncRNAs and mRNAs related to enriched signalling pathways were validated using quantitative polymerase chain reaction (qPCR).

Materials and methods

Ethical approval

This study was approved by the Institutional Review Board of the University of Hong Kong/ Hospital Authority Hong Kong West Cluster (reference no. UW19-140).

Primary cell culture

Human PDL cells were collected from five healthy teeth (i.e. no caries or periodontal disease) of five systematically healthy, non-smoking adults (two men and three women; age range: 18–33 years). The teeth were extracted due to orthodontic reasons. PDL cells were isolated from the PDL tissues using the tissue explanation outgrowth method as described by Somerman *et al*. and Feng *et al*., with minor modifications (15, 16). Specifically, after extraction, the tooth was gently rinsed with phosphate-buffered saline (PBS) to remove blood and debris. The PDL tissue was scraped gently from the middle third of the root surface using a scalpel to avoid contamination with the gingiva or dental pulp. Next, the PDL tissues were minced to yield small fragments, placed in a cell and tissue culture flask (surface area: 75 cm^2; Biofil, Guangzhou, China), and incubated for 1 hour at 37°C. Then, the explants were cultured in α-Modified Eagle's Medium supplemented with 10% (v/v) foetal bovine serum, 100 U/ml penicillin, and 0.1 mg/ml streptomycin (henceforth denoted as standard medium) and incubated at 37°C in an atmosphere with 5% carbon dioxide. The medium was replaced every 2–3 days with fresh standard medium. After PDL cells had grown out to confluence around the explants (approximately 10–14 days), they were passaged (p1) and cultured in a new flask until confluence was reached. Then the cells were trypsinized and passaged at 1:3 ratio. Experiments were performed using cells at the second (p2) or third (p3) passage.

Application of tensile loading

The cultured PDL cells were subjected to mechanical tensile loading *in vitro* using the Flexcell® 5000 tension system (Flexcell, Burlington, North Carolina, USA). In brief, cells were seeded onto flexible-bottomed BioFlex® (Flexcell) 6-well culture plates at a density of 2×10^5 cells/well and cultured until they reached 80% confluence. After a 12-hour period of serum starvation, the cells were subjected to static waves of 12% equibiaxial tensile strain using a computer-controlled vacuum stretch apparatus (17). PDL cells in the control group were cultured under the same conditions in the absence of tensile loading. Cells were subjected to tensile loading for 12 hours or 3 days for qPCR and western blotting, respectively, and continued to culture for 10 days prior to Alizarin Red S staining (ARS).

Characterization of cell surface markers

The surface markers expressed on PDL cells were characterized by flow cytometry. Briefly, PDL cells were harvested, then washed with PBS. Next, the cells were re-suspended in PBS to yield a single-cell suspension at a cell density of 10^7 cells per ml. One hundred microlitres of this suspension (1×10^6 PDL cells) were incubated with 3% bovine serum albumin and then labelled with fluorochrome-tagged anti-human monoclonal antibodies (all BD Pharmingen, San Diego, California, USA): CD73 (cat no. 561254, tag: fluorescein isothiocyanate), CD90 (cat no. 561557, peridinin chlorophyll protein), CD105 (cat no. 562408, allophycocyanin), or CD45 (cat no. 555483, phycoerythrin). The antibodies were diluted to the concentrations recommended by the manufacturer. After incubation at room temperature in the dark for 30 minutes, the cells were washed three times with PBS and immediately analysed using a FACSVerse flow cytometer (BD Biosciences, San Jose, California, USA).

Western blotting

PDL cells were lysed in radioimmunoprecipitation assay buffer (Thermo Fisher Scientific, Waltham, Massachusetts, USA) supplemented with a protease inhibitor cocktail (Halt, Thermo Fisher Scientific). The protein concentrations in the lysates were determined quantitatively using a Pierce BCA protein assay kit (Thermo Fisher Scientific). The proteins were then separated via sodium dodecyl sulphate–polyacrylamide gel electrophoresis on 10% (w/v) Tris-glycine gels (Bio-Rad, USA), followed by transfer onto polyvinylidene difluoride membranes. The blotted membranes were then blocked with Tris-buffered saline containing 5% (w/v) skimmed milk and 0.05% (v/v) Tween-20 at room

temperature for 1 hour. Specific antigens were immunodetected using appropriate primary and secondary antibodies and visualized using Pierce ECL Western Blotting Substrate (Thermo Fisher Scientific). Primary antibodies specific for runt-related transcription factor 2 (RUNX2; ab23981, Abcam, Cambridge, UK), collagen type I (COL1; PA5-95137; Thermo Fisher Scientific), and glyceraldehyde 3-phosphate dehydrogenase (GAPDH; 2118S; Cell Signaling Technology, Beverly, Massachusetts, USA) were used at dilutions of 1:1000. Horseradish peroxidase-conjugated goat anti-rabbit immunoglobulin G (7074S; Cell Signaling Technology) was used as the secondary antibody at a dilution of 1:3000. Finally, the intensities of the labelled protein bands were analysed using ImageJ software (National Institutes of Health, Bethesda, Maryland, USA).

Alizarin Red S staining

To characterize the differentiation potential, PDL cells were cultured in 6-well plates in osteogenic induction medium (10 nM dexamethasone, 10 mM β-glycerophosphate, and 50 μg/ml ascorbic acid; Sigma Aldrich) for 10 days. Subsequently, ARS was performed to evaluate calcium mineralization in the cultures after osteogenic induction. The cultured cells were fixed with 10% (w/v) formaldehyde, washed with deionized water, and stained with 1% (w/v) ARS solution (Sigma Aldrich) for 20 minutes at room temperature. After removing the ARS solution, the cultures were thoroughly washed with deionized water and subjected to digital imaging to visualize the stained calcium nodules within the cultures. The staining was then quantified using an osteogenesis quantitation kit (ECM815, Sigma Aldrich). The absorbance in each well was then measured at 405 nm on a SpectraMAX M2 microplate reader (Molecular Devices, Sunnyvale, California, USA), and the results were calculated using a standard curve.

RNA extraction and qPCR

Total RNA was extracted from cultured cells using the RNeasy Cell Mini Kit (Qiagen), and the RNA concentration in each sample was measured on a NanoDrop 2000 Spectrophotometer (Thermo Fisher Scientific). Total RNA (1 μg) was then reverse-transcribed to yield cDNA using the SuperScript™ III (Invitrogen, Carlsbad, California, USA). Next, qPCR analyses were performed using a StepOnePlus Real-Time PCR System (Applied Biosystems, Thermo Fisher Scientific) with fast SYBR Green Master Mix (Applied Biosystems, Thermo Fisher Scientific). The detailed protocol was provided in Supplementary Table 1. As suggested by Nazet *et al.*, TATA-box-binding protein (*TBP*) and peptidylprolyl isomerase B (*PPIB*; also known as cyclophilin B), when used in conjunction, are the most reliable reference genes for normalization in a qPCR analysis of PDL cells subjected to tensile loading (18). Therefore, the relative expression values were determined using the standard curve method and normalized to the expression of *TBP* and *PPIB*. The calculations were performed using R software. qPCR was performed and the results reported according to the Minimum Information for Publication of Quantitative Real-Time PCR Experiments (MIQE) guidelines (Supplementary Table 1) (19). The primer sequences corresponding to the target genes are shown in Supplementary Table 2.

High-throughput RNA-seq

PDL cells from each tooth (n = 5) were cultured and exposed or not to tensile loading for 12 hours. Next, the 10 cell samples (5 tension-loaded and 5 non-loaded controls) were subjected to high-throughput RNA-seq. RNA integrity was determined using an Agilent 2100 Bioanalyzer (Agilent Technologies Inc., Santa Clara, California, USA). For the 10 samples, the RNA integrity number (RIN) range was 9.8–10 (average RIN = 9.94). Four micrograms of RNA were extracted from each sample, and ribosomal RNA (rRNA) was depleted using the Epicentre Ribo-zero™ rRNA Removal Kit (Epicentre, Madison, Wisconsin, USA). The RNA library was prepared using the NEBNext Ultra™ Directional RNA Library Prep Kit for Illumina (New England Biolabs, Ipswich, Massachusetts, USA) in accordance with the manufacturer's recommendations. Paired-end sequencing of the library was performed using the NovaSeq 6000 system (Illumina). After sequencing, the raw data in FASTQ format were processed to remove adapter sequences and low-quality reads. The sequencing reads were then aligned to the human genome GRCh38 using HISAT2 (20). Finally, FeatureCount was used to retrieve the reads mapped to each gene and generate the expression count matrix (21). The raw data of the RNA-seq experiment have been deposited in the Gene Expression Omnibus database (accession no. GSE173891).

Bioinformatics analysis

Differential expression analysis was conducted using the R package Deseq2. *P*-Values or false discovery rates were adjusted using the Benjamini–Hochberg method (22). Genes with adjusted *P*-values <0.05 between the tension-loaded and control samples were considered to be differentially expressed. GO and KEGG pathway enrichment analyses of the differentially expressed genes were performed using the R package Clusterprofiler (23). GO terms and KEGG pathways with adjusted *P*-values <0.05 between the two conditions were considered significantly enriched. In addition, the Pearson correlation coefficients of lncRNA–mRNA and lncRNA–lncRNA pairs were calculated on the basis of their expression values. Co-expressed lncRNA–mRNA and lncRNA–lncRNA pairs with an absolute Pearson correlation coefficient $|r| \geq 0.9$ were selected and used to establish a co-expression network using the Cytoscape software (version 3.8.1; www.cytoscape.org). The mRNAs identified in the network were subjected to a GO analysis of function using ShinyGO v0.61 (adjusted $P < 0.05$) (24).

Statistics

The statistical analysis was performed using SPSS 25.0 software (IBM, Armonk, New York, USA) and GraphPad Prism 7 software (GraphPad Software Inc., San Diego, California, USA). Independent and paired Student's *t*-tests were used to compare the differences in results between the tension-loaded and the control groups. A significance level of $P < 0.05$ was set for all statistical analyses.

Results

Tensile loading enhanced the osteogenic potential of PDL cells

The flow cytometry analysis revealed that the isolated PDL cells were positive for the mesenchymal stem cell-related markers CD73, CD90, and CD105 and negative for the haematopoiesis-related marker CD45 (Supplementary Figure 1). The results of qPCR and western blotting analyses, respectively, suggested that the mRNA and protein levels of the osteogenic markers RUNX2 and COL1 were significantly higher in PDL cells subjected to tensile loading than in the controls (Figure 1A and B; Supplementary

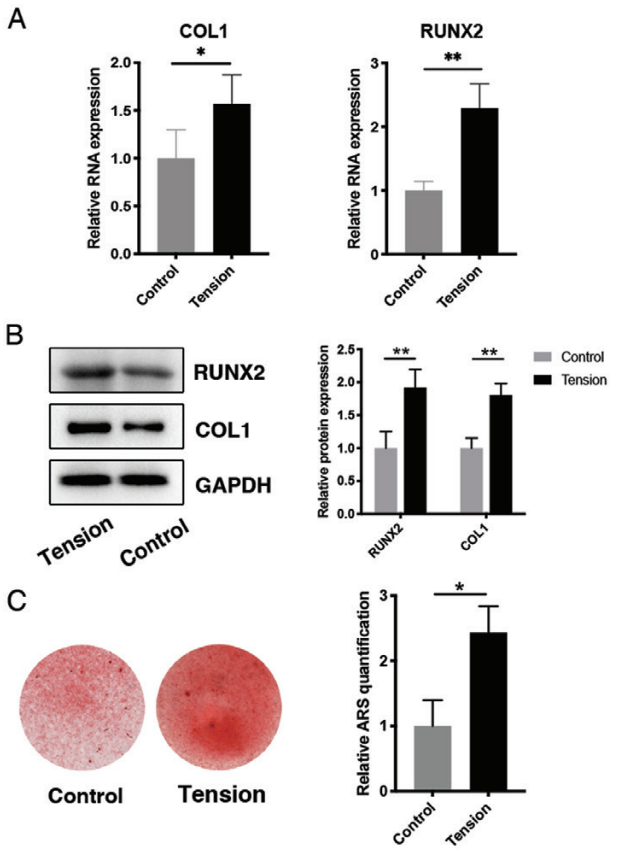

Figure 1. Tensile loading enhanced the osteogenic differentiation of human periodontal ligament (PDL) cells. (A) Quantitative polymerase chain reaction (qPCR) analysis of the relative mRNA expression of collagen type I (*COL1*) and runt-related transcription factor 2 (*RUNX2*) in PDL cells subjected or not to tensile loading for 12 hours. The results are normalized to the expression of TATA-box-binding protein (*TBP*) and peptidylprolyl isomerase B (*PPIB*) and expressed as means ± standard deviations. (B) Western blot analysis and relative quantification of COL1 and RUNX2 proteins in PDL cells subjected or not to tensile loading for 3 days. (C) Visualization and relative quantification of Alizarin Red S staining (ARS) in PDL cells subjected or not to tensile loading. $*P < 0.05$, $**P < 0.01$.

Figure 2). ARS revealed the increased formation of mineralized nodules in the tension-loaded cultured cells relative to the control cells (Figure 1C).

Differential expression of mRNAs and lncRNAs in PDL cells under tensile loading

Each pair of tension-loaded and non-loaded samples was compared in a pairwise manner ($n = 5$). Collectively, 1438 mRNAs (860 up- and 578 down-regulated) and 195 lncRNAs (107 up- and 88 down-regulated) were identified as differentially expressed (adjusted $P < 0.05$) in the tension group relative to the control group. Among these, 159 mRNAs (62 up- and 97 down-regulated) and 89 lncRNAs (48 up- and 41 down-regulated) had an absolute fold change >1.5. The top 10 up- and down-regulated mRNAs and lncRNAs are shown in Table 1. The differentially expressed mRNAs and lncRNAs were visualized by volcano plots (Figure 2A). A hierarchical clustering heap showing the expression profiles of the top 500 up- and top 500 down-regulated genes revealed significant differences in the expression profiles between the tension and control groups (Figure 2B).

GO and KEGG pathway enrichment analyses

All differentially expressed mRNAs were subjected to GO and KEGG pathway enrichment analyses. The GO results indicated that these mRNAs were enriched in all three biological aspects, namely biological process (BP), molecular function (MF), and cellular component (CC), with significant enrichment of 428, 36, and 14 items in these aspects, respectively (all adjusted $P < 0.05$). Ossification (GO: 0001503, adjusted $P = 1.65 \times 10^{-5}$) was the most significantly enriched BP term, with 79 mRNAs. Focal adhesion (GO: 0005925, adjusted $P = 1.35 \times 10^{-8}$) was the most significantly enriched CC term, with 84 mRNAs, and actin binding (GO: 0003779, adjusted $P = 1.59 \times 10^{-5}$) was the most significantly enriched MF term, with 85 mRNAs. The top 20 enriched GO terms are shown in Figure 3A.

In the KEGG pathway analysis, 35 pathways were found to be significantly enriched (all adjusted $P < 0.05$). The top six pathways associated with signal transduction were the phosphatidylinositol 3-kinase–protein kinase B (PI3K–Akt) signalling pathway (hsa04151, adjusted $P = 0.01$), insulin signalling pathway (hsa04910, adjusted $P = 2.70 \times 10^{-3}$), mammalian target of rapamycin (mTOR) signalling pathway (hsa04150, adjusted $P = 0.01$), Hippo signalling pathway (hsa04390, adjusted $P = 0.01$), Forkhead box O (FoxO) signalling pathway (hsa04068, adjusted $P = 2.70 \times 10^{-3}$), and hypoxia-inducible factor (HIF)-1 signalling pathway (hsa04066, adjusted $P = 2.22 \times 10^{-4}$). The top 15 enriched KEGG pathways are shown in Figure 3B.

Validation of differentially expressed mRNAs and lncRNAs

Three differentially expressed lncRNAs (*CYTOR*, *MIR22HG*, and *SNHG3*) and five differentially expressed mRNAs [epidermal growth factor receptor (*EGFR*), fibroblast growth factor 5 (*FGF5*), vascular endothelial growth factor A (*VEGFA*), HIF-1 subunit alpha (*HIF1A*), and *FOXO1*] associated with the significantly enriched pathways were selected for qPCR analyses. Compared with the control group, the expression levels of all three differentially expressed lncRNAs and four of the five differentially expressed mRNAs (*EGFR*, *FGF5*, *HIF1A*, and *VEGFA*) were significantly increased, whereas the expression level of *FOXO1* mRNA was significantly decreased in the tension group relative to the control group (Figure 4). These results were consistent with the RNA-seq results.

LncRNA–mRNA and lncRNA–lncRNA co-expression analyses

To predict the functions of the validated lncRNAs, we performed correlation analyses of the three validated lncRNAs (*MIR22HG*, *SNHG3*, and *CYTOR*) with all other differentially expressed genes. We calculated the Pearson correlation coefficients of all pairs of samples and selected those with an $|r| \geq 0.9$ to construct the co-expression network (Figure 5). We identified 126 pairs of lncRNA–mRNA or lncRNA–lncRNA. The results of the GO analyses showed that the co-expressed mRNAs of *MIR22HG*, *SNHG3*, and *CYTOR* were significantly enriched in several functions, of which regulation of response to stimulus, cellular component biogenesis and cell adhesion were top-ranked, respectively. The full list of enriched GO categories is provided in Supplementary Table 3.

Discussion

In this study, PDL cells were subjected to tensile loading to mimic clinical OTM in response to tensile strain placed on the stretched

Table 1. Top 10 up-regulated and down-regulated mRNAs and lncRNAs in PDL cells under tensile loading.

Ensemble ID	Gene symbol	Fold change	Adjusted *P*-value	Description
Up-regulated mRNAs				
ENSG00000139318	DUSP6	2.56	2.06E–52	Dual specificity phosphatase 6
ENSG00000120738	EGR1	1.94	9.44E–42	Early growth response 1
ENSG00000144136	SLC20A1	1.75	8.76E–26	Solute carrier family 20 (phosphate transporter), member 1
ENSG00000125740	FOSB	3.34	8.76E–26	FBJ murine osteosarcoma viral oncogene homolog B
ENSG00000138166	DUSP5	1.64	4.43E–25	Dual specificity phosphatase 5
ENSG00000112715	VEGFA	1.68	3.77E–23	Vascular endothelial growth factor A
ENSG00000159399	HK2	1.73	2.32E–21	Hexokinase 2
ENSG00000164056	SPRY1	1.81	6.09E–21	Sprouty homolog 1
ENSG00000143878	RHOB	1.67	4.42E–20	Ras homolog family member B
ENSG00000134363	FST	1.69	2.79E–18	Follistatin
Down-regulated mRNAs				
ENSG00000142632	ARHGEF19	0.54	5.60E–26	Rho guanine nucleotide exchange factor (GEF) 19
ENSG00000149212	SESN3	0.63	1.21E–22	Sestrin 3
ENSG00000109906	ZBTB16	0.66	2.58E–19	Zinc finger and BTB domain containing 16
ENSG00000198963	RORB	0.62	2.79E–18	RAR-related orphan receptor B
ENSG00000128335	APOL2	0.71	3.45E–17	Apolipoprotein L, 2
ENSG00000188177	ZC3H6	0.57	8.50E–17	Zinc finger CCCH-type containing 6
ENSG00000150907	FOXO1	0.63	1.83E–13	Forkhead box O1
ENSG00000120693	SMAD9	0.55	1.01E–12	SMAD family member 9
ENSG00000131386	GALNT15	0.59	3.63E–12	Polypeptide *N*-acetylgalactosaminyltransferase 15
ENSG00000168209	DDIT4	0.53	4.44E–11	DNA-damage-inducible transcript 4
Up-regulated lncRNAs				
ENSG00000286458	AC083870.1	1.97	4.69E–17	
ENSG00000222041	CYTOR	1.46	1.02E–09	Cytoskeleton regulator RNA
ENSG00000242125	SNHG3	1.39	1.05E–09	Small nucleolar RNA host gene 3
ENSG00000245573	BDNF-AS	1.51	2.06E–09	Brain derived neurotrophic factor—antisense RNA
ENSG00000257497	AC121761.1	2.36	2.75E–09	
ENSG00000253837	AC090197.1	1.85	1.42E–08	
ENSG00000238273	AC108058.1	1.53	5.12E–08	
ENSG00000257298	AC008147.2	1.66	1.30E–07	
ENSG00000286341	AP002762.3	1.65	1.81E–06	
ENSG00000172965	MIR4435-2HG	1.36	2.35E–06	MIR4435-2 host gene
Down-regulated lncRNAs				
ENSG00000226604	PAPPA-AS2	0.48	2.55E–08	Pappalysin 1—antisense RNA 2
ENSG00000272668	AL590560.3	0.54	3.90E–07	
ENSG00000250903	GMDS-DT	0.72	5.51E–06	GMDS divergent transcript
ENSG00000253320	AZIN1-AS1	0.50	7.08E–06	AZIN1 antisense RNA 1
ENSG00000205181	LINC00654	0.66	2.29E–05	Long intergenic non-protein-coding RNA 654
ENSG00000232855	AF165147.1	0.59	2.77E–05	
ENSG00000239828	AC063944.1	0.59	3.23E–05	
ENSG00000255364	SMILR	0.68	7.05E–05	Smooth muscle induced lncRNA
ENSG00000248932	AC046134.2	0.50	1.61E–04	
ENSG00000283175	AC007920.2	0.48	2.52E–04	

lncRNA, long non-coding RNA; mRNA, messenger RNA; PDL, periodontal ligament.

side. A previous report indicated that 12% elongation is optimal for increasing the proliferation and osteogenic potential of PDL cells (17). Our results show that the osteogenic activity of PDL cells was enhanced by tensile loading, as demonstrated by the increased expression of osteogenic markers and mineralized nodules.

Over time, considerable research has explored the regulatory mechanisms of OTM, and PDL cells subjected to mechanical loading are used widely to mimic *in vivo* conditions. Several microarray analyses have been performed to investigate the transcriptomes of PDL cells subjected to compressive or tensile forces. For example, de Araujo *et al.* applied compressive force to PDL cells and identified 85 up-regulated and 23 down-regulated genes (25). Specifically, signal transduction proteins such as Ras homologue gene family member E (RhoE), a major regulator of cytoskeleton dynamics and cell morphology and mobility, were significantly up-regulated in compressed PDL cells. Wescott *et al.* reported 16 genes that exhibited significant changes in expression in response to a 12% uniaxial cyclic tensile strain (13). More recently, Chang *et al.* used a microarray analysis to identify 818 mRNAs and 32 microRNAs that were differentially expressed in cyclic tension-induced PDL cells relative to control cells (26). However, the signalling pathways and regulatory mechanisms associated with this mechano-chemical transduction process remain elusive.

The recent development of RNA-seq offers an unprecedented potential for transcriptome characterization and therefore can be used as an extensive tool for elucidating genes and metabolic pathways involved in various biological processes. RNA-seq has advantages over traditional microarrays. In particular, it is more accurate and provides more comprehensive information about the characteristics of transcripts, is not limited to the known genes represented on a microarray and can detect novel transcription variants via alternative splicing (27).

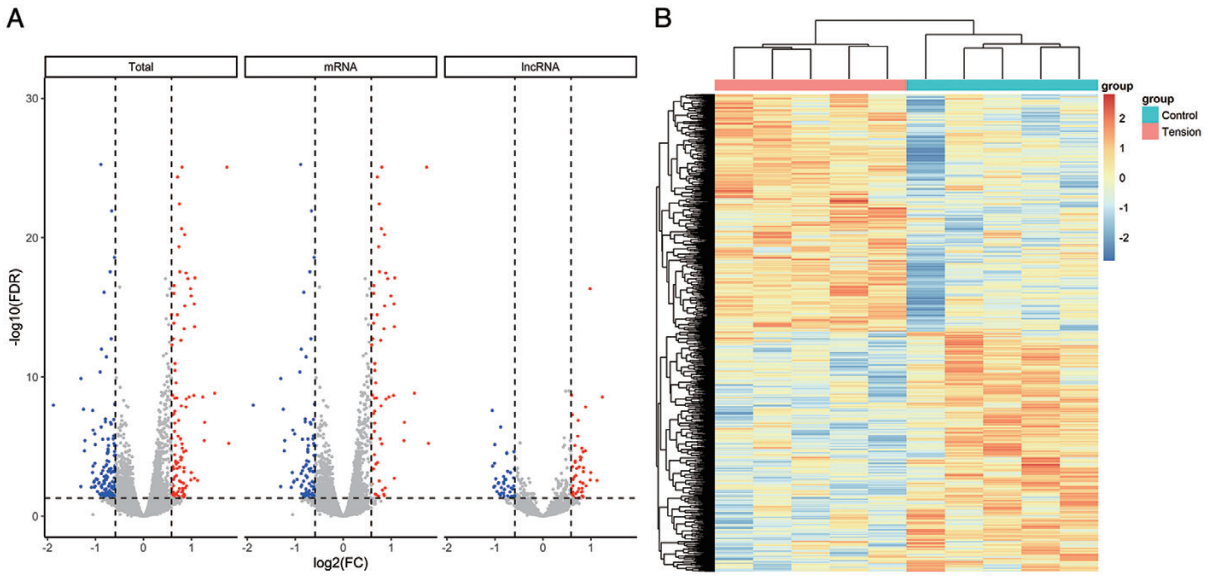

Figure 2. Differentially expressed mRNAs and long non-coding RNAs (lncRNAs) in PDL cells under tensile loading. (A) Volcano plot of the distributions of differentially expressed mRNAs and lncRNAs (adjusted *P*-value <0.05). Red dots indicate up-regulated mRNAs or lncRNAs with fold changes ≥1.5; blue dots indicate down-regulated mRNAs or lncRNAs with fold changes ≤0.667. FC, fold change; FDR, false discovery rate; PDL, periodontal ligament. (B) Clustering heatmap of the top 500 up-regulated and 500 down-regulated genes (mRNAs and lncRNAs). Each column represents one sample, and each row represents one differentially expressed gene.

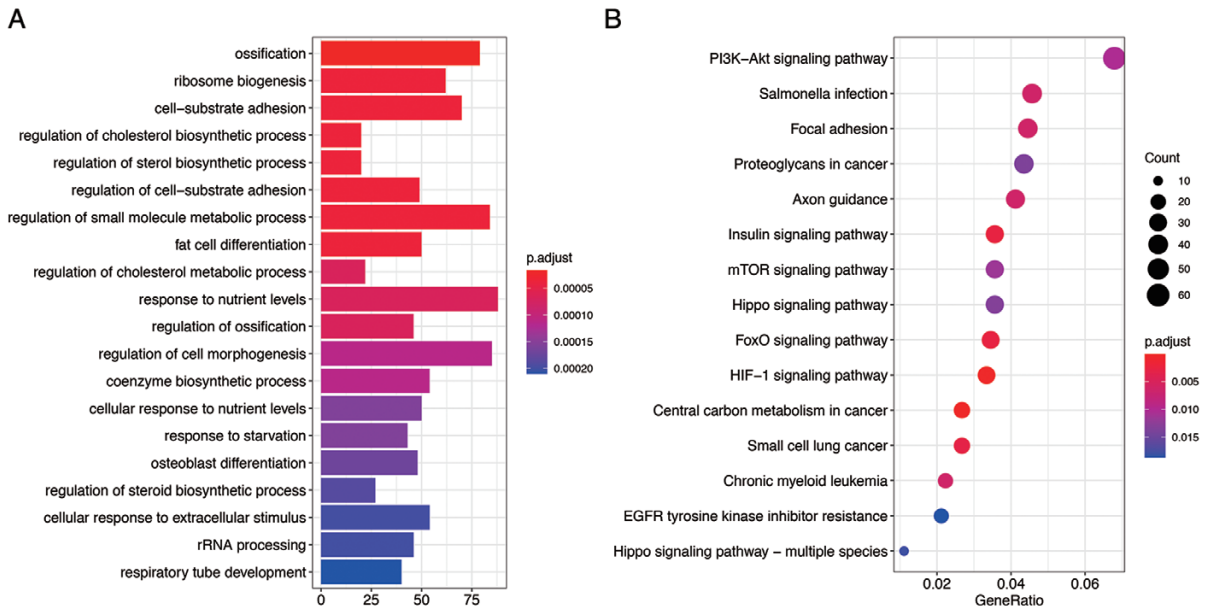

Figure 3. Gene Ontology (GO) and Kyoto Encyclopedia of Genes and Genomes (KEGG) pathway enrichment analyses. (A) Top 20 enriched GO terms of differentially expressed genes. (B) Top 15 enriched KEGG pathways of differentially expressed genes.

Non-coding RNAs have received much attention as regulators in a variety of diseases and biological processes. LncRNAs can affect gene expression both directly and indirectly in various biological processes. However, the mechanism by which tensile loading affects lncRNA expression in PDL cells remains unclear. In a recent study, Wang *et al*. also reported differentially expressed genes in PDL cells subjected to tensile loading (28). However, their analyses of the enriched functions indicated by these differentially expressed genes yielded considerably different results compared with our analyses. These differences might be largely attributable to differences in the samples. We performed RNA-seq on 10 samples from 5 individuals and conducted paired analyses in our differential expression analysis, whereas Wang *et al*. used two mixed samples from different subjects (28). The discrepancy in the results might also be explained by differences in the level of equibiaxial strain applied to the PDL cells, which was 12% in our study and 10% in the study by Wang *et al*. (28). Differences in library preparation, sequencing techniques, and analysis methods between the studies might also have led to differences in the results.

In our study, PDL cells were collected from the extracted teeth of five healthy individuals, cultured separately, and loaded with tensile force. We then used RNA-seq to thoroughly elucidate the

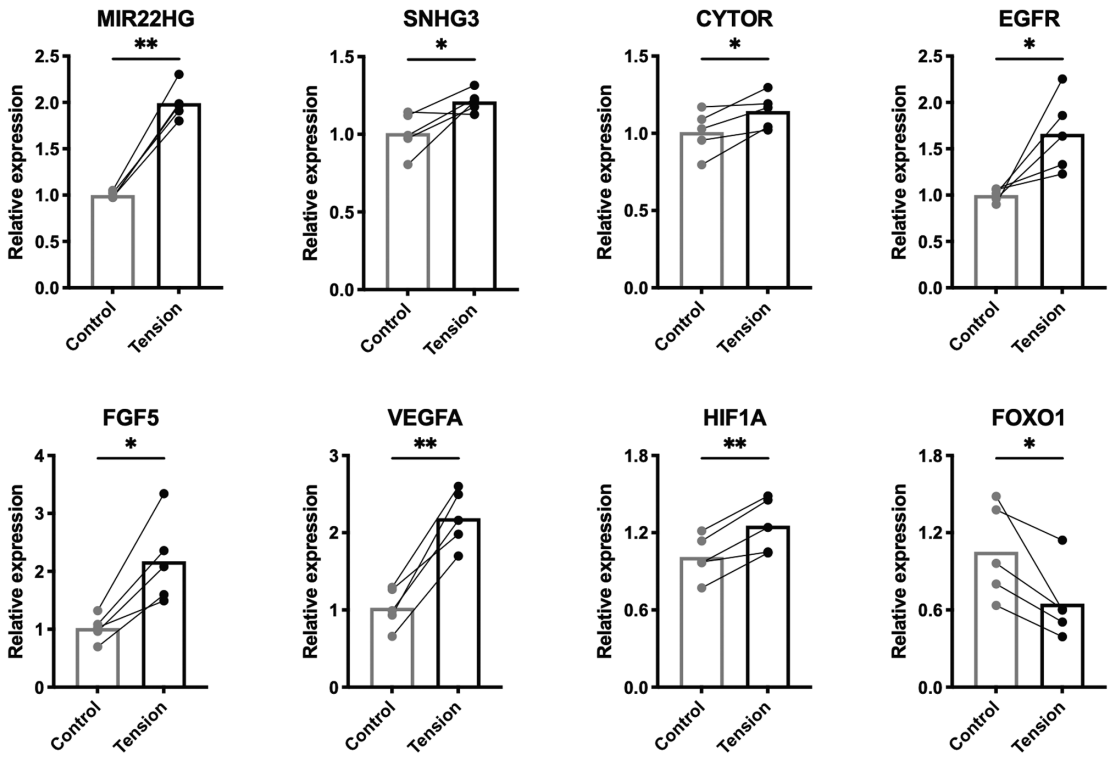

Figure 4. qPCR validation of the expression of three lncRNAs (*MIR22HG*, *SNHG3*, and *CYTOR*) and five mRNAs [epidermal growth factor receptor (*EGFR*), fibroblast growth factor 5 (*FGF5*), vascular endothelial growth factor A (*VEGFA*), hypoxia-inducible factor 1 subunit alpha (*HIF1A*), and Forkhead box O1 (*FOXO1*)] identified as differentially expressed in the RNA sequencing analysis. The results were normalized to the expression of *TBP* and *PPIB*. The paired Student's *t*-test was used to conduct the statistical analyses (**P* < 0.05, ***P* < 0.01). lncRNAs, long non-coding RNAs; *PPIB*, peptidylprolyl isomerase B; qPCR, quantitative polymerase chain reaction; *TBP*, TATA-box-binding protein.

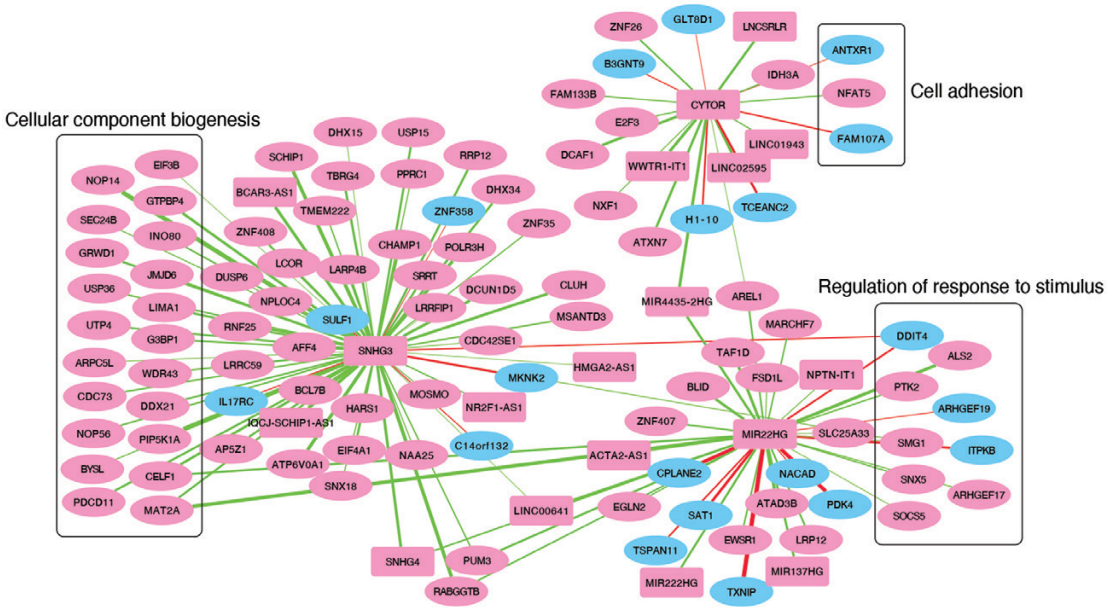

Figure 5. LncRNA and mRNA co-expression network. A co-expression network of three validated lncRNAs (*CYTOR*, *MIR22HG*, and *SNHG3*) associated with other differentially expressed lncRNAs and mRNAs (Pearson correlation coefficient ≥0.9) was constructed. Elliptical nodes represent mRNAs; rectangular nodes represent lncRNAs. Up- and down-regulation are represented by pink and blue colours, respectively. Green lines represent positive correlations; red lines represent negative correlations. The thickness of the line indicates the strength of the correlation.

lncRNA and mRNA expression profiles of the tension-loaded and non-loaded PDL cells. Collectively, we identified 1438 and 195 differentially expressed mRNAs and lncRNAs, respectively, in the tension group relative to the control group, suggesting that these genes might contribute to the mechano-chemical transduction of PDL cells. The expression of three up-regulated lncRNAs—*CYTOR*,

SNHG3, and *MIR22HG*—was further validated by qPCR analysis. These three lncRNAs have been reported to play an important role in various cancers, including colon cancer, liver cancer, and lung cancer (29–31). In our study of PDL cells under tensile stimulation, the co-expression analysis revealed that *CYTOR*, *SNHG3*, and *MIR22HG* were co-expressed with genes associated with cell adhesion, cellular component biogenesis, and regulation of response to stimulus, respectively, suggesting that these lncRNAs play important roles in these processes. Recently, *MIR22HG* was shown to participate in the osteogenic differentiation of PDL cells and bone marrow mesenchymal stem cells (BMSCs) (32, 33). It was suggested that *MIR22HG* could enhance the osteogenic differentiation of BMSCs, whereas *MIR22HG* knockdown could suppress this process (33).

The results of our GO analysis indicated the enrichment of a broad spectrum of biological processes, cellular components and molecular functions in response to tensile loading. Of the top 20 enriched GO terms, ossification, regulation of ossification, and osteoblast differentiation are related to bone formation. This observation is consistent with the increased osteogenic potential observed in the tension group relative to the control group.

The top enriched signalling pathways included the PI3K–Akt, mTOR, Hippo, FoxO, and HIF-1 pathways. The PI3K–Akt pathway is an intracellular signal transduction pathway that exerts central regulatory roles in metabolism, cell cycle, proliferation, differentiation, and angiogenesis in response to extracellular signals (34). PI3K–Akt signalling reportedly contributes to the osteogenesis of mesenchymal stem cells (34, 35). Specifically, PI3K–Akt signalling contributes integrally to RUNX2-dependent osteoblast differentiation by enhancing DNA binding of RUNX2 and RUNX2-dependent transcription (35). Furthermore, Song *et al*. reported that cyclic mechanical stress significantly activated the PI3K–Akt pathway and enhanced the expression of RUNX2 and COL1 in BMSCs (36). Activation of EGFR and FGF5 may lead to the downstream PI3K signalling pathway and subsequently enhance metabolism and cell growth (34, 37). Our RNA-seq results revealed increased expression of *EGFR* and *FGF5* in the tension group, thus supporting the role of the PI3K–Akt pathway in the tension-induced osteogenesis of PDL cells. Interestingly, the lncRNA *MIR22HG* was recently reported to enhance osteogenesis in BMSCs via the PI3K–Akt pathway (33). Further studies are warranted to elucidate the role of *MIR22HG* in tension-induced osteogenesis through the PI3K–Akt pathway.

Additionally, the PI3K–Akt pathway may exhibit crosstalk with the mTOR and FoxO signalling cascades. FoxO-mediated signal transduction regulates a wide range of cellular processes, including angiogenesis, differentiation, metabolism, stress resistance, and cell cycle (38). Evidence suggests that FoxO proteins can attenuate osteogenesis by suppressing the Wnt signalling pathway (39). Liu *et al*. suggested the involvement of FoxO signalling in the response of cementoblasts subjected to compressive loading (40). In our study, the expression of FoxO1 was significantly reduced in the tension-loaded group, and this might have contributed to the increase in bone formation. This finding further strengthens the evidence supporting a role for FoxO signalling in the mechano-chemical transduction process that occurs during OTM. The mTOR pathway is a key regulator of metabolism and physiology and plays important regulatory roles in cell growth, proliferation, apoptosis, and protein synthesis (41). The mTOR signalling pathway has been reported to participate in cellular responses to fluid shear stress and compression loading (40, 42). HIF, a crucial mediator of oxygen homeostasis and cellular adaptation to hypoxic conditions, facilitates the recruitment and differentiation of multipotent mesenchymal stem cells (43). Hypoxia can activate the HIF-1 signalling pathway to stimulate VEGF production and thereby enhance osteogenesis and angiogenesis (44, 45). By applying negative intermittent negative pressure to BMSCs, Yang *et al*. demonstrated increases in the levels of VEGF and bone formation, which were mediated by HIF-1 (46). In our study, we demonstrated increased *HIF1A* and *VEGF* expression in the tension-loaded group relative to the control, suggesting that HIF-1 signalling might participate in tension-induced osteogenesis in PDL cells. In short, despite increasing research interest in regulation of lncRNAs in bone remodelling in recent years, most current studies have only explored *in vitro* models at the cellular level. More in-depth *in vivo* exploration is certainly warranted.

Conclusions

This RNA-seq-based study elucidated changes in the lncRNA and mRNA expression profiles of PDL cells subjected to tensile loading, and revealed differentially expressed genes and significantly enriched signal transduction pathways. In PDL cells, these signalling pathways were responsive to tensile loading and might therefore participate in bone remodelling during OTM. Further studies are needed to validate these intracellular signal transduction mechanisms underlying tension-induced bone remodelling in PDL cells and the potential regulatory effects of lncRNAs.

Supplementary material

Supplementary material is available at *European Journal of Orthodontics* online.

Supplementary Figure 1. Flow cytometry analysis of the mesenchymal stem cell-related markers CD73, CD90, and CD105 and the haematopoiesis-related marker CD45 on PDL cells.

Supplementary Figure 2. Original western blots of COL1, RUNX2, and GAPDH in PDL cells exposed or not to tensile loading.

Supplementary Table 1. Minimum Information for Publication of Quantitative Real-Time PCR Experiments (MIQE) checklist.

Supplementary Table 2. Primer sequences used in quantitative polymerase chain reactions.

Supplementary Table 3. Enriched Gene Ontology categories identified in the analysis of co-expressed mRNAs in the lncRNA–mRNA co-expression network.

Funding

This work was supported by the Hong Kong Research Grants Council (GRF no. 17106619) and the Seed Fund for Basic Research of the University of Hong Kong (no. 201904185012).

Conflicts of interest

None to declare.

Data availability

Raw data of the RNA-seq experiment have been deposited in the Gene Expression Omnibus database (accession no. GSE173891).

References

1. Long, P., Liu, F., Piesco, N.P., Kapur, R. and Agarwal, S. (2002) Signaling by mechanical strain involves transcriptional regulation of proinflammatory genes in human periodontal ligament cells in vitro. *Bone*, 30, 547–552.

2. Diercke, K., Sen, S., Kohl, A., Lux, C.J. and Erber, R. (2011) Compression-dependent up-regulation of ephrin-A2 in PDL fibroblasts attenuates osteogenesis. *Journal of Dental Research*, 90, 1108–1115.
3. Kim, S.J., Park, K.H., Park, Y.G., Lee, S.W. and Kang, Y.G. (2013) Compressive stress induced the up-regulation of M-CSF, RANKL, TNF-α expression and the down-regulation of OPG expression in PDL cells via the integrin-FAK pathway. *Archives of Oral Biology*, 58, 707–716.
4. Yoo, J.H., Lee, S.M., Bae, M.K., Lee, D.J., Ko, C.C., Kim, Y.I. and Kim, H.J. (2018) Effect of orthodontic forces on the osteogenic differentiation of human periodontal ligament stem cells. *Journal of Oral Science*, 60, 438–445.
5. Esteller, M. (2011) Non-coding RNAs in human disease. *Nature Reviews. Genetics*, 12, 861–874.
6. Taft, R.J., Pang, K.C., Mercer, T.R., Dinger, M. and Mattick, J.S. (2010) Non-coding RNAs: regulators of disease. *The Journal of Pathology*, 220, 126–139.
7. He, Q., Yang, S., Gu, X., Li, M., Wang, C. and Wei, F. (2018) Long noncoding RNA TUG1 facilitates osteogenic differentiation of periodontal ligament stem cells via interacting with Lin28A. *Cell Death & Disease*, 9, 1–14.
8. Salmena, L., Poliseno, L., Tay, Y., Kats, L. and Pandolfi, P.P. (2011) A ceRNA hypothesis: the Rosetta Stone of a hidden RNA language? *Cell*, 146, 353–358.
9. Lin, Y., Jin, L., Tong, W.M., Leung, Y.Y., Gu, M. and Yang, Y. (2021) Identification and integrated analysis of differentially expressed long non-coding RNAs associated with periodontitis in humans. *Journal of Periodontal Research*, doi: 10.1111/jre.12864.
10. Gu, X., Li, M., Jin, Y., Liu, D. and Wei, F. (2017) Identification and integrated analysis of differentially expressed lncRNAs and circRNAs reveal the potential ceRNA networks during PDLSC osteogenic differentiation. *BMC Genetics*, 18, 100.
11. Peng, W., Deng, W., Zhang, J., Pei, G., Rong, Q. and Zhu, S. (2018) Long noncoding RNA ANCR suppresses bone formation of periodontal ligament stem cells via sponging miRNA-758. *Biochemical and Biophysical Research Communications*, 503, 815–821.
12. Huang, Y., Zhang, Y., Li, X., Liu, H., Yang, Q., Jia, L., Zheng, Y. and Li, W. (2019) The long non-coding RNA landscape of periodontal ligament stem cells subjected to compressive force. *European Journal of Orthodontics*, 41, 333–342.
13. Wescott, D.C., Pinkerton, M.N., Gaffey, B.J., Beggs, K.T., Milne, T.J. and Meikle, M.C. (2007) Osteogenic gene expression by human periodontal ligament cells under cyclic tension. *Journal of Dental Research*, 86, 1212–1216.
14. Wu, Y., Ou, Y., Liao, C., Liang, S. and Wang, Y. (2019) High-throughput sequencing analysis of the expression profile of microRNAs and target genes in mechanical force-induced osteoblastic/cementoblastic differentiation of human periodontal ligament cells. *American Journal of Translational Research*, 11, 3398–3411.
15. Feng, F., Akiyama, K., Liu, Y., Yamaza, T., Wang, T.M., Chen, J.H., Wang, B.B., Huang, G.T., Wang, S. and Shi, S. (2010) Utility of PDL progenitors for in vivo tissue regeneration: a report of 3 cases. *Oral Diseases*, 16, 20–28.
16. Somerman, M.J., Archer, S.Y., Imm, G.R. and Foster, R.A. (1988) A comparative study of human periodontal ligament cells and gingival fibroblasts in vitro. *Journal of Dental Research*, 67, 66–70.
17. Liu, J., Li, Q., Liu, S., Gao, J., Qin, W., Song, Y. and Jin, Z. (2017) Periodontal ligament stem cells in the periodontitis microenvironment are sensitive to static mechanical strain. *Stem Cells International*, 2017, 1380851.
18. Nazet, U., Schröder, A., Spanier, G., Wolf, M., Proff, P. and Kirschneck, C. (2020) Simplified method for applying static isotropic tensile strain in cell culture experiments with identification of valid RT-qPCR reference genes for PDL fibroblasts. *European Journal of Orthodontics*, 42, 359–370.
19. Bustin, S.A., et al. (2009) The MIQE guidelines: minimum information for publication of quantitative real-time PCR experiments. *Clinical Chemistry*, 55, 611–622.
20. Kim, D., Paggi, J.M., Park, C., Bennett, C. and Salzberg, S.L. (2019) Graph-based genome alignment and genotyping with HISAT2 and HISAT-genotype. *Nature Biotechnology*, 37, 907–915.
21. Liao, Y., Smyth, G.K. and Shi, W. (2014) featureCounts: an efficient general purpose program for assigning sequence reads to genomic features. *Bioinformatics (Oxford, England)*, 30, 923–930.
22. Benjamini, Y. and Hochberg, Y. (1995) Controlling the false discovery rate: a practical and powerful approach to multiple testing. *Journal of the Royal Statistical Society: Series B (Methodological)*, 57, 289–300.
23. Yu, G., Wang, L.G., Han, Y. and He, Q.Y. (2012) clusterProfiler: an R package for comparing biological themes among gene clusters. *OMICS*, 16, 284–287.
24. Ge, S.X., Jung, D. and Yao, R. (2020) ShinyGO: a graphical gene-set enrichment tool for animals and plants. *Bioinformatics (Oxford, England)*, 36, 2628–2629.
25. de Araujo, R.M., Oba, Y. and Moriyama, K. (2007) Identification of genes related to mechanical stress in human periodontal ligament cells using microarray analysis. *Journal of Periodontal Research*, 42, 15–22.
26. Chang, M., Lin, H., Luo, M., Wang, J. and Han, G. (2015) Integrated miRNA and mRNA expression profiling of tension force-induced bone formation in periodontal ligament cells. *In Vitro Cellular & Developmental Biology. Animal*, 51, 797–807.
27. Wang, Z., Gerstein, M. and Snyder, M. (2009) RNA-Seq: a revolutionary tool for transcriptomics. *Nature Reviews. Genetics*, 10, 57–63.
28. Wang, H., Feng, C., Li, M., Zhang, Z., Liu, J. and Wei, F. (2021) Analysis of lncRNAs-miRNAs-mRNAs networks in periodontal ligament stem cells under mechanical force. *Oral Diseases*, 27, 325–337.
29. Su, W., et al. (2018) Silencing of long noncoding RNA MIR22HG triggers cell survival/death signaling via oncogenes YBX1, MET, and p21 in lung cancer. *Cancer Research*, 78, 3207–3219.
30. Yue, B., Liu, C., Sun, H., Liu, M., Song, C., Cui, R., Qiu, S. and Zhong, M. (2018) A positive feed-forward loop between LncRNA-CYTOR and Wnt/beta-catenin signaling promotes metastasis of colon cancer. *Molecular Therapy*, 26, 1287–1298.
31. Zhang, P.F., Wang, F., Wu, J., Wu, Y., Huang, W., Liu, D., Huang, X.Y., Zhang, X.M. and Ke, A.W. (2019) LncRNA SNHG3 induces EMT and sorafenib resistance by modulating the miR-128/CD151 pathway in hepatocellular carcinoma. *Journal of Cellular Physiology*, 234, 2788–2794.
32. Zheng, Y., Li, X., Huang, Y., Jia, L. and Li, W. (2018) Time series clustering of mRNA and lncRNA expression during osteogenic differentiation of periodontal ligament stem cells. *PeerJ*, 6, e5214.
33. Jin, C., Jia, L., Tang, Z. and Zheng, Y. (2020) Long non-coding RNA MIR22HG promotes osteogenic differentiation of bone marrow mesenchymal stem cells via PTEN/AKT pathway. *Cell Death & Disease*, 11, 1–13.
34. Chen, J., Crawford, R., Chen, C. and Xiao, Y. (2013) The key regulatory roles of the PI3K/Akt signaling pathway in the functionalities of mesenchymal stem cells and applications in tissue regeneration. *Tissue Engineering. Part B, Reviews*, 19, 516–528.
35. Fujita, T., Azuma, Y., Fukuyama, R., Hattori, Y., Yoshida, C., Koida, M., Ogita, K. and Komori, T. (2004) Runx2 induces osteoblast and chondrocyte differentiation and enhances their migration by coupling with PI3K-Akt signaling. *The Journal of Cell Biology*, 166, 85–95.
36. Song, F., Jiang, D., Wang, T., Wang, Y., Lou, Y., Zhang, Y., Ma, H. and Kang, Y. (2017) Mechanical stress regulates osteogenesis and adipogenesis of rat mesenchymal stem cells through PI3K/Akt/GSK-3β/β-catenin signaling pathway. *BioMed Research International*, 2017, 6027402.
37. Ornitz, D.M. and Itoh, N. (2015) The fibroblast growth factor signaling pathway. *Wiley Interdisciplinary Reviews. Developmental Biology*, 4, 215–266.
38. Calnan, D.R. and Brunet, A. (2008) The FoxO code. *Oncogene*, 27, 2276–2288.
39. Iyer, S., Ambrogini, E., Bartell, S.M., Han, L., Roberson, P.K., de Cabo, R., Jilka, R.L., Weinstein, R.S., O'Brien, C.A. and Manolagas, S.C. (2013) FOXOs attenuate bone formation by suppressing Wnt signaling. *The Journal of Clinical Investigation*, 123, 3409–3419.
40. Liu, H., Huang, Y., Zhang, Y., Han, Y., Zhang, Y., Jia, L., Zheng, Y. and Li, W. (2019) Long noncoding RNA expression profile of mouse cementoblasts under compressive force. *The Angle Orthodontist*, 89, 455–463.

41. Laplante, M. and Sabatini, D.M. (2009) mTOR signaling at a glance. *Journal of Cell Science*, 122, 3589–3594.
42. Qi, L. and Zhang, Y. (2014) The microRNA 132 regulates fluid shear stress-induced differentiation in periodontal ligament cells through mTOR signaling pathway. *Cellular Physiology and Biochemistry*, 33, 433–445.
43. Wagegg, M., et al. (2012) Hypoxia promotes osteogenesis but suppresses adipogenesis of human mesenchymal stromal cells in a hypoxia-inducible factor-1 dependent manner. *PLoS One*, 7, e46483.
44. Schipani, E., Maes, C., Carmeliet, G. and Semenza, G.L. (2009) Regulation of osteogenesis-angiogenesis coupling by HIFs and VEGF. *Journal of Bone and Mineral Research*, 24, 1347–1353.
45. Wang, Y., et al. (2007) The hypoxia-inducible factor alpha pathway couples angiogenesis to osteogenesis during skeletal development. *The Journal of Clinical Investigation*, 117, 1616–1626.
46. Yang, Z., et al. (2014) Functions and mechanisms of intermittent negative pressure for osteogenesis in human bone marrow mesenchymal stem cells. *Molecular Medicine Reports*, 9, 1331–1336.